Electromagnetic Waves Over Half-Space Metamaterials of Arbitrary Permittivity and Permeability

Akira Ishimaru, *Life Fellow, IEEE*, John Rhodes Thomas, and Sermsak Jaruwatanadilok

***Abstract*—Most electromagnetic problems deal with media with unit permeability. However, recent interest in metamaterials necessitated studies of wave characteristics in media with arbitrary permittivity and permeability whose real parts can be positive or negative. This paper presents analysis of wave characteristics on semiinfinite metamaterials. Waves are excited by electric or magnetic line sources, and the problem is separated into the p (TM) and the s (TE) polarization, showing symmetries. The Fourier spectra of the reflection and transmission coefficients are examined and the poles, branch points, and zeros are shown in the real μ-real ϵ diagram. We clarify the location of poles in proper and improper Riemann Surfaces, and the excitation of forward and backward surface waves, forward and backward Lateral waves, and Zenneck waves, and the relations between Brewster's angle and Sommerfeld poles. We include the behaviors of the backward surface waves and the temporal backward Lateral waves.**

***Index Terms*—Brewster's angle, lateral waves, metamaterials, negative index, permeability, permittivity, surface waves, Zenneck waves.**

I. Introduction

In recent years, there has been an increasing interest in development of new materials whose characteristics may not be found in nature [1]–[7]. Examples are metamaterials, in particular negative index materials (NIM), chiral media, and composite materials. A broad range of applications has been suggested including artificial dielectrics, lenses, absorbers, antenna structures, optical and microwave components, sensors, and frequency selective surfaces.

In the development of these materials, there are several important questions. We need to know how the waves behave in metamaterials, what characteristics may be useful for practical applications, how to construct such metamaterials, and what new applications can be identified to utilize new wave characteristics. This paper deals with the first of the above questions. Other questions have been considered and reported in special issues and other publications [6]–[9]. In conventional electromagnetics, the permeability is one ($\mu = \text{relative permeability} = 1$) except magnetic materials. In metamaterials, however, the real parts of μ and ϵ can range from $-\infty$ to $+\infty$, though the imaginary parts should always be negative in $\exp(j\omega t)$ representation for passive materials. This paper presents a study of wave excitation in semiinfinite metamaterials. This problem for ordinary materials with $\mu = 1$ has been studied extensively including the Sommerfeld poles, Zenneck waves, Brewster's angle, surface waves, and lateral waves. Now, since the permeability is no longer limited to one, many new waves and new phenomena emerge.

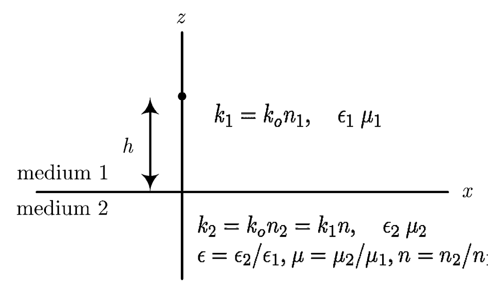

Fig. 1. Medium 1 is ordinary material, and both ϵ_1 and μ_1 are real and positive. Medium 2 is metamaterial with complex ϵ_2 and μ_2. ϵ, μ, and n are normalized with respect to medium 1. Line source is at $x = 0$ and $z = h$.

We first present a comprehensive analysis of all CW wave types. New wave types such as backward surface waves and backward lateral waves are discussed and the relationship between Brewster's angle and Zenneck wave is clarified. We include some discussions on pulse and wave packet propagation and time-dependent lateral waves. Our analysis is limited to 2-D problems with isotropic metamaterials. In general, however, metamaterials are anisotropic and highly dispersive, requiring further investigations [5]–[9].

II. Line Source Over a Semi-Infinite Metamaterial

We consider an electric or a magnetic line source located over a metamaterial as shown in Fig. 1.

For the p-polarization (TM), we have

$$\left(\frac{\partial^2}{\partial x^2} + \frac{\partial^2}{\partial z^2} + k_i^2\right) H_y = -(-j\omega\epsilon_1 I_m)\delta(x)\delta(z-h)$$
$$k_i^2 = k_o^2 \mu_i \epsilon_i \quad (1)$$

where I_m is the magnetic line current and we use the normalization $-j\omega\epsilon_1 I_m = 1, k_o$ is free space wavenumber, μ_i and ϵ_i are relative permeability and permittivity $(i = 1, 2)$.

Manuscript received March 4, 2004; revised September 8, 2004. This work was supported by the National Science Foundation under Grant ESC-9908849.
The authors are with the Department of Electrical Engineering, University of Washington, Seattle, WA 98195 USA (e-mail: ishimaru@ee.washington.edu).
Digital Object Identifier 10.1109/TAP.2004.842572

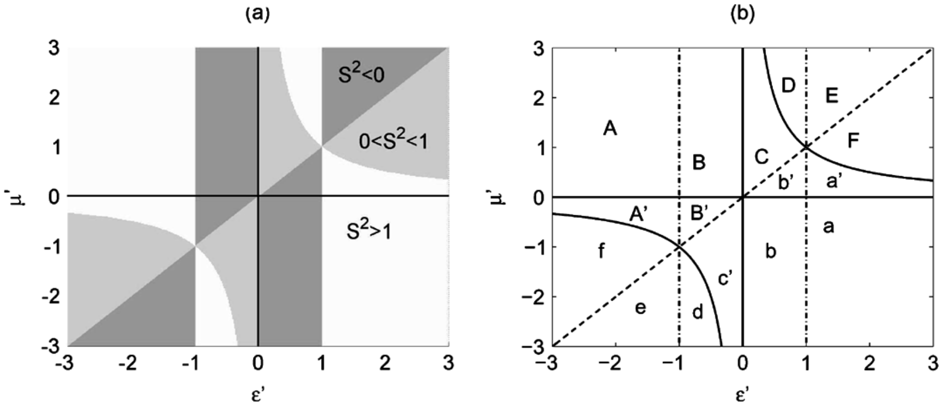

Fig. 2. (a) Regions of $S^2 > 1$ (white), $1 > S^2 > 0$ (gray), and $S^2 < 0$ (dark). (b) Different regions in μ'-ϵ' plane.

Using the boundary condition that H_y and $(1/\epsilon)(\partial/\partial z)H_y$ are continuous at $z = 0$, we get the well-known Fourier representation of the incident (H_{yi}), the reflected (H_{yr}) and the transmitted (H_{yt}) fields [11].

$$
\begin{aligned}
H_{yi} &= \frac{1}{2\pi}\int \frac{\exp(-jk_{z1}|z-h| - jk_x x)}{2jk_{z1}}dk_x \\
H_{yr} &= \frac{1}{2\pi}\int R(k_x)\frac{\exp(-jk_{z1}(z+h) - jk_x x)}{2jk_{z1}}dk_x \\
H_{yt} &= \frac{1}{2\pi}\int T(k_x)\frac{\exp(-jk_{z1}h + jk_{z2}z - jk_x x)}{2jk_{z1}}dk_x \quad (2)
\end{aligned}
$$

where $k_{zi} = \sqrt{k_i^2 - k_x^2}, R(k_x) = ((Z_1 - Z_2)/(Z_1 + Z_2))$, $T(k_x) = ((2Z_1)/(Z_1 + Z_2)), Z_i = ((k_{zi})/(\omega\epsilon_i)), Z_i$ is the wave impedance. First we note that for the s-polarization (TE), we have the same equation for E_y with the replacement of $(-j\omega\epsilon_1 I_m)$ by $(-j\omega\mu_1 I = 1)$. The boundary condition at $z = 0$ is the continuity of E_y and $(1/\mu)(\partial/\partial z)E_y$. Therefore the field for the s-polarization is identical to the field for the p-polarization with the interchange of μ_i and ϵ_i in both media.

III. Surface Waves and Lateral Waves

As preliminary to this analysis, we need to pay close attention to the square root of various quantities. For passive media, we require, with $\exp(j\omega t)$ time dependence $\Im(\mu_i) < 0$ and $\Im(\epsilon_i) < 0$ where $\Im$ denotes the *imaginary part of*. The refractive index $n = \sqrt{\mu\epsilon}$ needs to be chosen such that

$$\Im(n) = \Im(\sqrt{\mu\epsilon}) < 0. \quad (3)$$

From (3), it follows that the characteristic impedance Z_{oi} and admittance Y_{oi} must have positive real parts, where $Z_{oi} = (1)/(Y_{oi}) = Z_o\sqrt{(\mu_i)/(\epsilon_i)}, Z_o = \sqrt{(\mu_o)/(\epsilon_o)}$.

Next, k_{zi} needs to be chosen carefully. From the branch points at $k_x = k_i$ in the complex k_x plane, we draw the branch cuts along $\Im(k_{zi}) = 0$. Then, in the top surface of k_x plane, $\Im(k_{zi}) < 0$ and the wave attenuates as $|z| \to \infty$. Thus this is called the *proper Riemann surface*. Even though the branch cuts can be drawn in other ways, the above choice is most common [10]. In the *improper Riemann surfaces*, one or both $\Im(k_{zi})$ become positive [11].

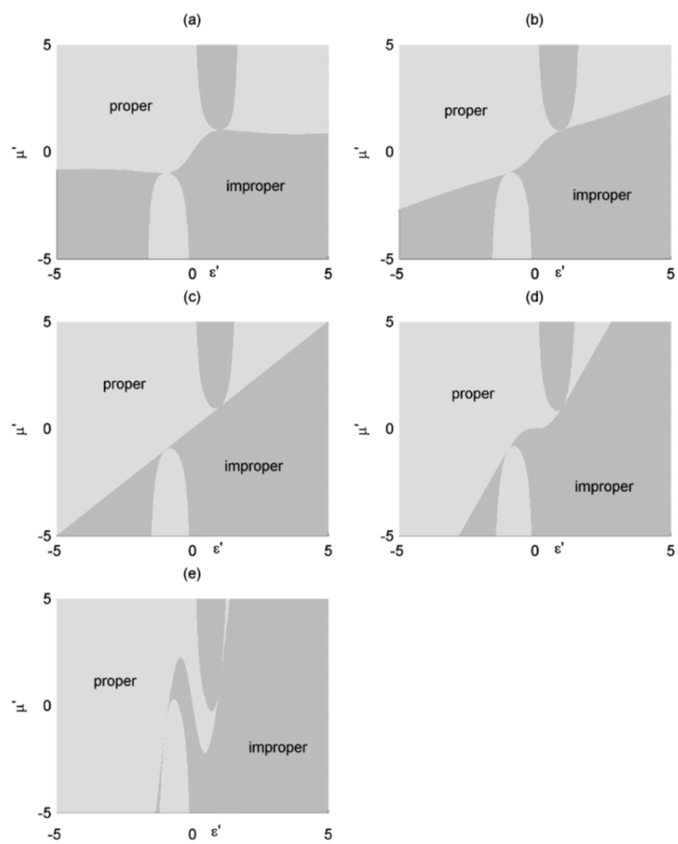

Fig. 3. Regions for $\Im(k_{z1}) < 0$ (proper) and $\Im(k_{z1}) > 0$ (improper) in the μ'-ϵ' plane. ϵ''/μ'' = (a) 10. (b) 2. (c) 1. (d) 0.5. (e) 0.1.

Let us examine the reflection coefficient $R(k_x)$

$$R(k_x) = \frac{(k_{z1}/\epsilon_1) - (k_{z2}/\epsilon_2)}{(k_{z1}/\epsilon_1) + (k_{z2}/\epsilon_2)}. \quad (4)$$

The zero and pole are given by

$$\frac{k_{z1}}{\epsilon_1} = \pm\frac{k_{z2}}{\epsilon_2} \qquad \begin{aligned} &+\text{Brewster's zero} \\ &-\text{Zenneck wave pole.}\end{aligned} \quad (5)$$

Solving for k_x, we get the pole at $k_x = k_{xp}$.

$$k_{xp} = k_1 S, \quad S^2 = \frac{\epsilon^2 - n^2}{\epsilon^2 - 1}, \quad \epsilon = \frac{\epsilon_2}{\epsilon_1}, \quad n = \frac{n_2}{n_1}. \quad (6)$$

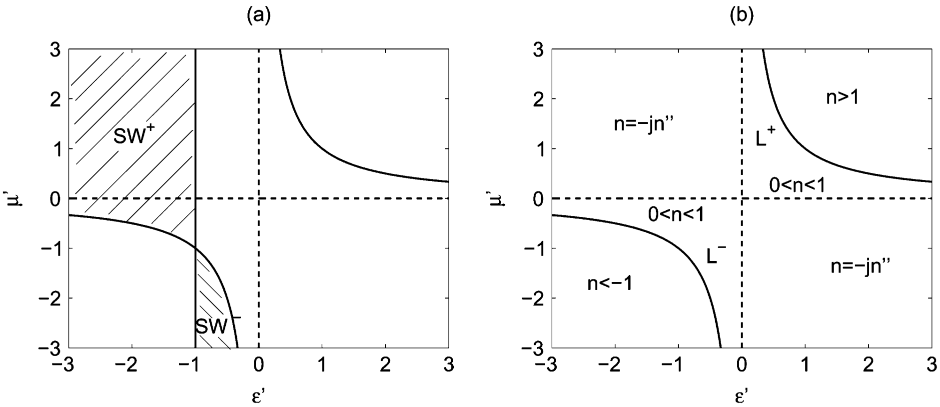

Fig. 4. (a) Forward surface waves SW^+ and backward surface waves SW^-. (b) Forward lateral waves L^+ and backward lateral waves L^- waves. NIM is in the third quadrant.

To verify whether the pole is in the proper Riemann surface, we first obtain

$$k_{z2} = \sqrt{k_2^2 - k_{xp}^2}. \tag{7}$$

The square root is taken such that $\Im(k_{z2}) < 0$.

We then calculate k_{z1} using (5)

$$k_{z1} = -\frac{\epsilon_1}{\epsilon_2} k_{z2} = -\frac{1}{\epsilon} k_{z2}. \tag{8}$$

If $\Im(k_{z1}) < 0$, the pole is in the *proper* Riemann surface (I), and if $\Im(k_{z1}) > 0$, the pole is in an *improper* Riemann surface (II). See [11].

Note that S^2 in (6) corresponds to both zero and pole in (4). Brewster's angle is when the reflection coefficient is zero and, therefore, the classification as pole or zero is based on (5). We will discuss this further later.

Let us now examine the location of the pole in the k_x-plane. For real ϵ and μ, S is pure real or pure imaginary so the pole $k_{xp} = k_1 S$ lies on the real or imaginary axis in the k_x-plane. Fig. 2 then shows the regions in the ϵ'-μ' plane where different wave types can exist.

If $S^2 > 1$, forward or backward surface waves can exist. If $0 < S^2 < 1$, there may be Zenneck waves, and if $S^2 < 0$, the poles are in the imaginary axis and the wave may be exponentially decaying along the surface.

However, this is not sufficient to describe the wave types. We also need to examine whether these poles are in the proper or improper Riemann surfaces by examining whether $\Im(k_{z1})$ is negative or positive with $\Im(k_{z2}) < 0$. However, this depends greatly upon the ratio of the imaginary parts of ϵ and μ. We write

$$\begin{aligned} \epsilon &= \epsilon' - j\epsilon'' \\ \mu &= \mu' - j\mu''. \end{aligned} \tag{9}$$

We show in Fig. 3, five cases where the ratio $\epsilon''/\mu'' = 10, 2, 1, 0.5, 0.1$.

In Fig. 2, there are four regions where $S^2 > 1$ and surface waves can exist. However, as shown in Fig. 3, the two regions (a and D) with $S^2 > 1$ on the right side ($\epsilon' > 0$) of Fig. 2 are in the improper Riemann surface. Hence, the surface wave can exist only in the region $\epsilon' < 0$ where the poles are in the proper Riemann surface. In fact, we will show that the forward and backward surface waves exist in the two regions shown in Fig. 4(a).We also note the forward L^+ and the backward L^- lateral waves can exist in region $1 > n > 0$ and $0 > n > -1$, respectively, [see Fig. 4(b)].

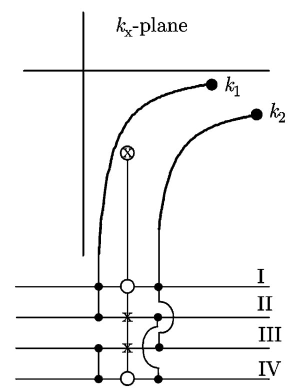

Fig. 5. Zenneck wave pole at o and Brewster's zero at x. Riemann surface I: $\Im(k_{z1}) < 0, \Im(k_{z2}) < 0$. II: $\Im(k_{z1}) > 0, \Im(k_{z2}) < 0$. III: $\Im(k_{z1}) < 0, \Im(k_{z2}) > 0$. IV: $\Im(k_{z1}) > 0, \Im(k_{z2}) > 0$.

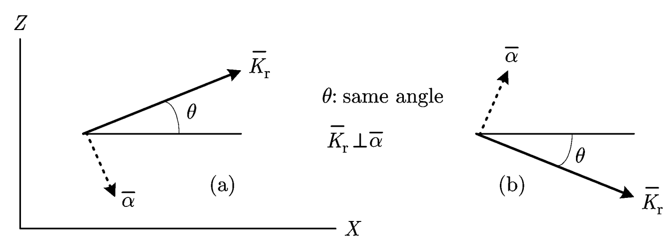

Fig. 6. Propagation constant k_{z1} at (a) Brewster's zero. (b) Zenneck wave pole.

IV. Brewster's Angle and Zenneck Wave

It has been known that Brewster's angle and Zenneck wave are closely related. However their relationship is often not clearly explained. We first note that at Brewster's angle, the reflection coefficient is zero while at the Zenneck wave pole (sometimes called the *Sommerfeld pole*), the reflection coefficient is infinite. Brewster's angle is normally defined for plane wave incidence on lossless dielectric material, but here, we generalized it to include a lossy medium and complex angle, and call it *Brewster's zero*. This terminology was included in (5).

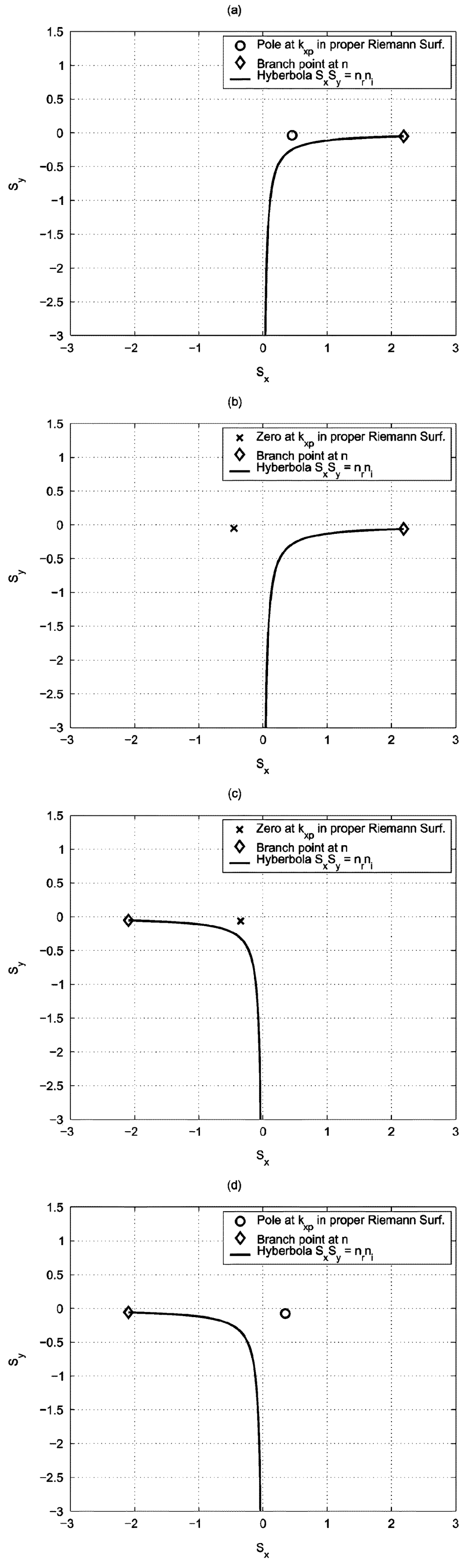

Fig. 7. Complex S-plane ($S = k_x/k_1$) plots of pole and branch cut to n for (a) case F_{10}: $\varepsilon = 2.4 - 0.1\mathrm{j}, \mu = 2 - 0.01\mathrm{j}, \Im(\varepsilon)/\Im(\mu) = 10$. (b) case $\mathrm{F}_{0.1}$: $\varepsilon = 2.4 - 0.01\mathrm{j}, \mu = 2 - 0.1\mathrm{j}, \Im(\varepsilon)/\Im(\mu) = 0.1$. (c) case f_{10}: $\varepsilon = -2.2 - 0.1\mathrm{j}, \mu = -2 - 0.01\mathrm{j}, \Im(\varepsilon)/\Im(\mu) = 10$. (d) case $\mathrm{f}_{0.1}$: $\varepsilon = -2.2 - 0.01\mathrm{j}, \mu = -2 - 0.1\mathrm{j}, \Im(\varepsilon)/\Im(\mu) = 0.1$.

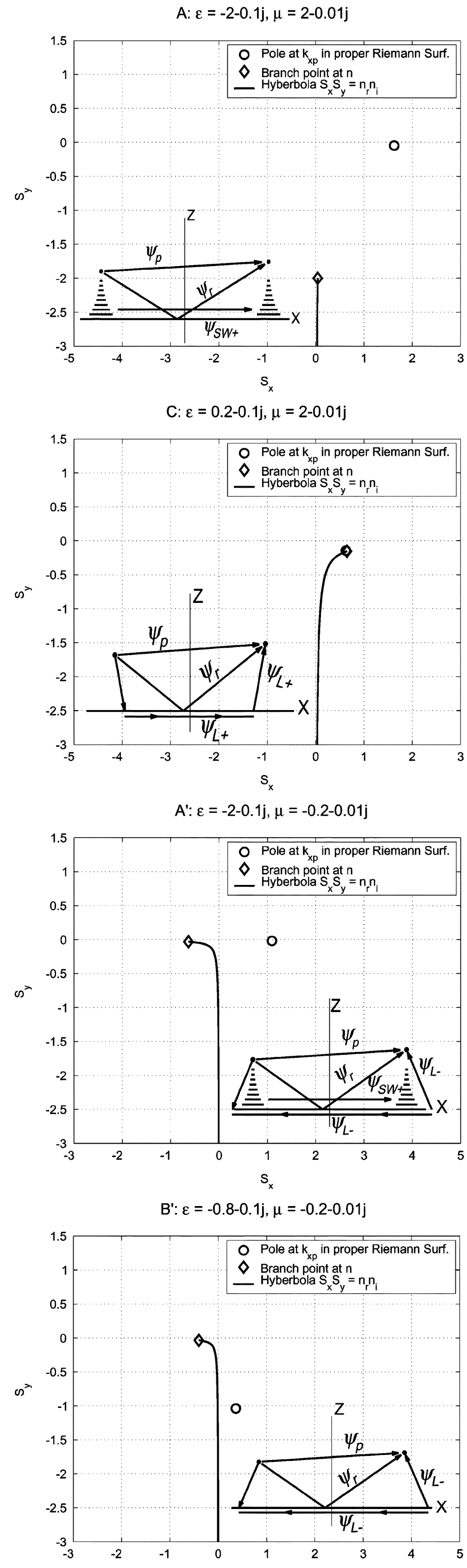

Fig. 8. Complex S-plane ($S = k_x/k_1$) plots of pole and branch cut to n for (ϵ, μ) cases in A, C, A′, B′ of Fig. 2(b) with illustration of resulting asymptotic wave types. Exponentially decaying horizontal lines represent the surface wave coupled from source to observation point.

Now at the Zenneck wave pole, we have

$$\Im(k_{z1}) < 0 \quad \text{and} \quad \Im(k_{z2}) < 0 \tag{10}$$

on Riemann surface I. At Brewster's zero, we have

$$\Im(k_{z1}) > 0 \quad \text{and} \quad \Im(k_{z2}) < 0 \tag{11}$$

on Riemann surface II.

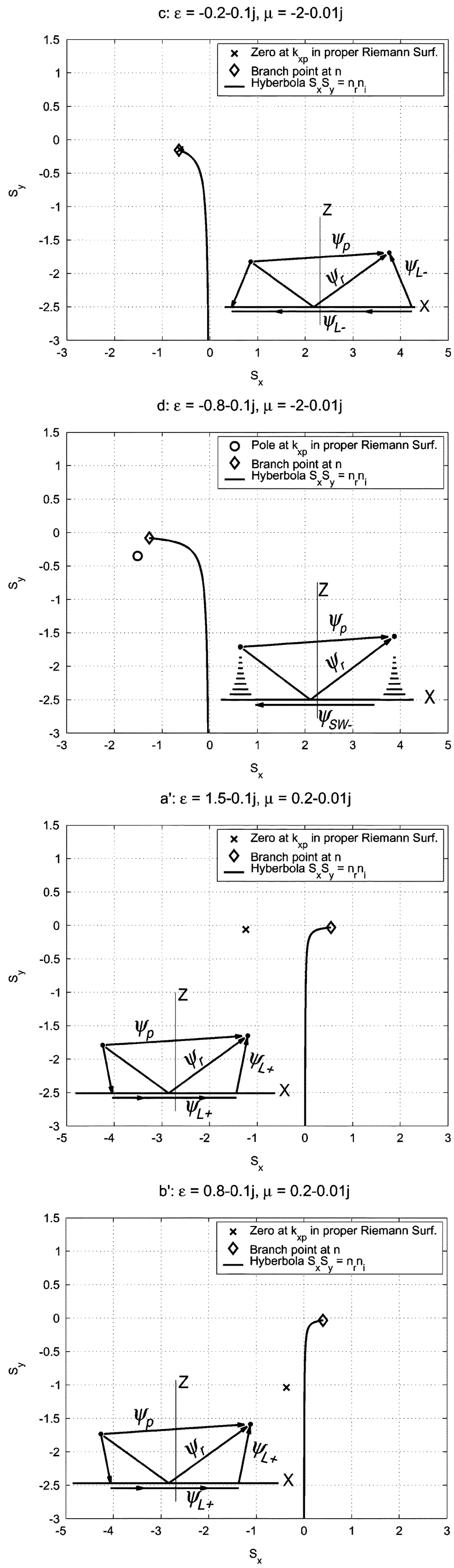

Fig. 9. Complex S-plane ($S = k_x/k_1$) plots of pole and branch cut to n for (ϵ, μ) cases in c, d, a′, b′ of Fig. 2(b) with illustration of resulting asymptotic wave types. Exponentially decaying horizontal lines represent the surface wave coupled from source to observation point.

In the k_x or S plane ($k_x = k_1 S$), both pole and zero are at the same point, but these two are on two different Riemann surfaces as shown in Fig. 5. Physically, the spectral factors associated with the reflected wave in (2) have the same propagation constant along the surface at Brewster's zero and Zenneck pole, but the phase front and the attenuation directions are different [11]. The exponent of the spectrum can be written as

$$\exp(-jk_{z1}z - jk_x x) = \exp(-j\bar{K}_r \cdot \bar{r} - \bar{\alpha} \cdot \bar{r}) \qquad (12)$$

where $\bar{K}_r$ and $\bar{\alpha}$ represent the phase front propagation and the attenuation direction, respectively, as shown in Fig. 6.

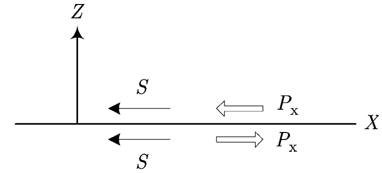

Fig. 10. Backward surface wave.

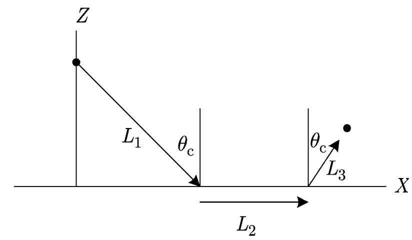

Fig. 11. Conventional forward lateral wave.

The pole and the zero in Fig. 5 are for a typical Sommerfeld problem of wave propagation over a conducting earth. For metamaterials, we need to reexamine Fig. 5.

We label different regions shown in Fig. 2(a) as in Fig. 2(b). Then, from Fig. 2(a), we note that $1 > S^2 > 0$ in Region C, F, c, f. However, we will see in the next section that the Zenneck wave occurs only in regions F and f. The boundaries of the regions shown in Fig. 2(b) represent the limits for $\epsilon'' \to 0$ and $\mu'' \to 0$. In computations for a large sample of cases covering Fig. 2(b), we have observed that for small imaginary parts these boundaries depend primarily on the ratio ϵ''/μ''.

The wave type in F and f depends on the ratio ϵ''/μ''. In Fig. 7, we show that Zenneck wave poles exist for $\mathrm{F}_{10}(\epsilon''/\mu'' = 10)$ and $\mathrm{f}_{0.1}(\epsilon''/\mu'' = 0.1)$, but not for $\mathrm{F}_{0.1}(\epsilon''/\mu'' = 0.1)$ and $\mathrm{f}_{10}(\epsilon''/\mu'' = 10)$. In Figs. 7–9, to reduce crowded lines, we do not show the branch cut from $S = (1,0)$ to $(0,0)$ to $(0,-\infty)$, which is the same cut from k_1 shown in Fig. 5. We have used the notation $S = S_x + jS_y$ in Figs. 7–9. In the legend, the symbol o or x denotes a pole or zero of S, respectively. The diamond represents the branch point at $S = n$. The symmetric branch cuts and branch points in the upper half of the k_x plane are not shown.

V. Wave Types in μ'-ϵ' Diagram—Examples

We have computed proper pole positions and branch cuts that determine the listed wave types for a large number of cases of (μ, ϵ). We have explored the variation with real parts as shown by regions in the μ'-ϵ' diagram, and we have explored variations with small negative imaginary parts. Our first calculations considered imaginary parts $\mathcal{O}(10^{-3})$ and we expanded to about 0.1.

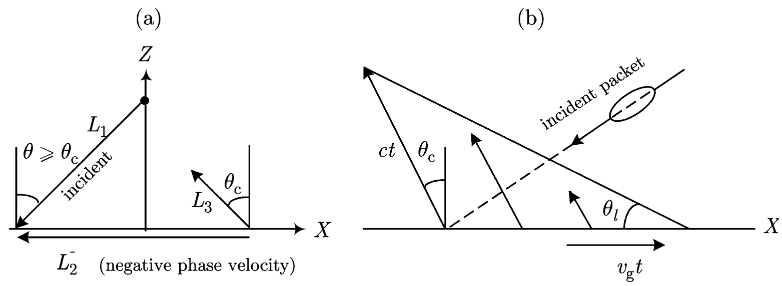

Fig. 12. (a) Backward lateral wave and (b) wave packet.

We noted that the boundary between regions of different wave type could change (e.g., region d expands with increasing ϵ'' to include a small part of region e where ϵ' is less than -1). We conclude that in the limit $\epsilon'' \to 0$ and $\mu'' \to 0$, the boundaries are as shown in Fig. 2(b), and the wave types by region are as follows:

A	forward surface wave (SW^+);
B	evanescent wave (E);
D and E	improper mode (Im)
F	Zenneck wave or improper mode;
A′	backward lateral wave (L^-), forward surface wave (SW^+);
B′	backward lateral wave (L^-);
a, b	improper mode (Im);
c	backward lateral wave (L^-);
d	backward surface wave (SW^-);
e	improper mode;
f	improper mode or Zenneck wave;
C, a′, b′	forward lateral wave (L^+).

We now show examples of various wave types for selected parts (not F nor f) of the μ'-ϵ' diagram [Fig. 2(b)]. These examples, shown in Figs. 8 and 9, are for the case of $\epsilon'' = 0.1$ and $\mu'' = 0.01$. We use these rather large values for small quantities so that the branch cut curves and poles lie far enough away from the axes to be readily visible. The choice of ϵ'' as larger than μ'' is partly motivated by our determination that ϵ'' is the controlling loss for our p-polarization (TM) case. However, the same wave type by region was found for other values that explored the range $0.1 \le \epsilon''/\mu'' \le 10$ and beyond. In each of these figures, we also show schematically the behaviors of the primary waves ψ_p, reflected waves ψ_r, surface waves ψ_{SW}, and lateral waves ψ_L in their asymptotic forms at large distance.

The usual dielectric range that produces Zenneck waves in Region F was illustrated in Fig. 7(a). The well-known surface wave (plasmon) for Region A is illustrated in Fig. 8 case A. The forward lateral wave that occurs in conventional electromagnetics with propagation from a medium of higher refractive index to one of lower index is illustrated in Fig. 8 case A′, Fig. 9 case a′ and Fig. 9 case b′.

VI. Backward Surface Waves

We have found a slow-wave pole (pole with $\Re(S_x) < -1$) occurs in region d of Fig. 2(b) [also SW^- in Fig. 4(a)]. An example of the pole and branch cut configuration is shown in Fig. 9 case d. For lossless cases, the phase velocity is in the negative x direction. However the Poynting vector in the medium 2 and medium 1 are pointed in $+x$ and $-x$ direction, respectively, and the total power is pointed in $+x$ direction. The Poynting vector in the x direction is given by

$$P_x = \frac{k_1 S}{2\omega\epsilon_o\epsilon_i}|H_y|^2 \quad \begin{cases} i=1 & \text{for medium1} \\ i=2 & \text{for medium 2.} \end{cases} \tag{13}$$

Since $S < -1, \epsilon_1$ is real and positive, and $-1 < \epsilon < 0$ in medium 2, $P_x < 0$ in medium 1 and $P_x > 0$ in medium 2. Furthermore, the total power in $+x$ direction is given by

$$\begin{aligned} P_{\text{total}} &= \int_0^\infty P_x dx + \int_{-\infty}^0 P_x\, dx \\ &= \frac{1}{4}\frac{S}{\omega\epsilon_o\epsilon_1}\frac{1}{\sqrt{S^2-1}}\left[1 - \frac{1}{\epsilon^2}\right] \end{aligned} \tag{14}$$

which becomes positive as expected as shown in Fig. 10.

VII. Backward Lateral Wave and Temporal Wave Packet

In Figs. 2(b), 8, and 9 the backward lateral wave is shown as occurring in NIM regions A′, B′, and c. A conventional forward lateral wave is pictured in Fig. 11.

The forward lateral wave is given by

$$H_y \propto \exp(-jk_1L_1 - jk_2L_2 - jk_1L_3) \tag{15}$$

and θ_c is the critical angle ($= \sin^{-1}(\Re(n))$). The backward lateral wave is given by the same expression, but $k_2 = k_1 n, 0 > n > -1$, and $\theta_c < 0$. This is pictured in Fig. 12(a).

It should, however, be noted that NIM is highly dispersive and, therefore, the wave in NIM over L_2 propagates with group velocity rather than phase velocity. If a wave packet is incident on NIM, the wave packet propagates as shown in Fig. 12(b). In this figure, the backward lateral wave emerges from a source point that travels along the x axis at group velocity v_g as shown. The lateral wave radiates into medium 1 (shown as freespace) at the critical angle θ_c. Then, θ_l represents the angle between the front of the lateral wave packet and the x axis.

The group refractive index n_g is given by

$$n_g = \frac{\partial}{\partial\omega}(n\omega) = \frac{c}{v_g}. \tag{16}$$

The law of sines applied to the triangle in Fig. 12(b) then gives [8]

$$\sin^2\theta_l = \frac{n_g^2(1-|n|^2)}{1+2n_g|n|+n_g^2}. \tag{17}$$

Exact numerical calculation of the space-time wave packet confirms this behavior of the backward lateral wave [8].

VIII. Conclusion

Conventional electromagnetics deals with media whose permeability is one, except magnetic materials. If the permeability can take any arbitrary value, this greatly expands the scope of electromagnetics resulting in a variety of complex new wave phenomena. This paper considers a line source excitation over a semiinfinite metamaterial. Careful attention is paid to poles and zeros in different Riemann surfaces, and new wave types including backward surface wave and backward lateral wave are discussed including the effects of dispersion.

References

[1] V. G. Veselago, "The electrodynamics of substances with simultaneously negative values of ϵ and μ," *Sov. Phy. Usp.*, vol. 10, no. 4, pp. 509–514, Jan.–Feb. 1968.

[2] J. B. Pendry, A. J. Holden, D. J. Robbins, and W. J. Stewart, "Magnetism from conductors and enhanced nonlinear phenomena," *IEEE Trans. Microw. Theory Tech.*, vol. 47, no. 11, pp. 2075–2084, Nov. 1999.

[3] D. R. Smith, W. J. Padilla, D. C. Vier, S. C. Nemat-Nasser, and S. Schultz, "Composite medium with simultaneously negative permeability and permittivity," *Phys. Rev. Lett.*, vol. 84, no. 18, pp. 4184–4187, May 2000.

[4] J. B. Pendry, "Negative refraction makes a perfect lens," *Phy. Rev. Lett.*, vol. 85, no. 18, pp. 3966–3969, Oct. 2000.

[5] R. W. Ziolkowski and E. Heyman, "Wave propagation in media having negative permittivity and permeability," *Phy. Rev. E*, vol. 64, no. 5, pp. 056625-01–056625-15, 2001.

[6] A. Ishimaru, S.-W. Lee, and Y. Kuga, "Generalized constitutive relations for metamaterials based on the quasistatic lorentz theory," *IEEE Trans. Antennas Propag.*, vol. 51, no. 10, pp. 2550–2557, Oct. 2003.

[7] A. Ishimaru, S. Jaruwatanadilok, and Y. Kuga, Generalized surface plasmon resonance sensors using metamaterials and negative index materials, in Pregress in electromagnetic research, Special Issue on Metamaterials, Elsevier, New York, pp. 139–152, 2005.

[8] A. Ishimaru and J. R. Thomas, "Waves in layered negative index media excited by space-time localized source," in *Proc. URSI Int. Symp. Electromagnetics Theory*, Pisa, Italy, May 2004.

[9] "Special issue on metamaterials," *IEEE Trans. Antennas Propag.*, vol. 51, no. 10, pp. 2546–2547, Oct. 2003.

[10] L. B. Felsen and N. Marcuvitz, *Radiation and Scattering of Waves*. New York: IEEE, 1994.

[11] A. Ishimaru, *Electromagnetic Wave Propagation, Radiation and Scattering*. Englewood Cliffs, NJ: Prentice-Hall, 1991.

Akira Ishimaru (M'58–SM'63–F'73–LF'94) received the B.S. degree in 1951 from the University of Tokyo, Tokyo, Japan, and the Ph.D. degree in electrical engineering in 1958 from the University of Washington, Seattle.

From 1951 to 1952, he was with the Electrotechnical Laboratory, Tanashi, Tokyo, and in 1956, he was with Bell Laboratories, Holmdel, NJ. In 1958, he joined the faculty of the Department of Electrical Engineering, University of Washington, where he was a Professor of electrical engineering and an Adjunct Professor of applied mathematics. He is currently Professor Emeritus there. He has also been a Visiting Associate Professor with the University of California, Berkeley. His current research includes waves in random media, remote sensing, object detection, and imaging in clutter environment, inverse problems, millimeter wave, optical propagation and scattering in the atmosphere and the terrain, rough surface scattering, optical diffusion in tissues, and metamaterials. He is the author of *Wave Propagation and Scattering in Random Media* (NewYork: Academic, 1978; IEEE-Oxford University Press Classic reissue, 1997) and *Electromagnetic Wave Propagation, Radiation, and Scattering* (EnglewoodCliffs, NJ: Prentice-Hall, 1991).

Dr. Ishimaru was Editor (1979–1983) of *Radio Science* and Founding Editor of *Waves in Random Media*, Institute of Physics, U.K. He has served as a member-at-large of the U.S. National Committee (USNC) and was chairman (1985–1987) of Commission B of the USNC/International Union of Radio Science. He is a Fellow of the Optical Society of America, the Acoustical Society of America, and the Institute of Physics, U.K. He was the recipient of the 1968 IEEE Region VI Achivement Award and the IEEE Centennial Medal in 1984. He was appointed as Boeing Martin Professor in the College of Engineering in 1993. In 1995, he was awarded the Distinguished Achievement Award from the IEEE Antennas and Propagataion Society. He was elected to the National Academy of Engineering in 1996. In 1998, he was awarded the Distinguished Achievement Award from the IEEE Geoscience and Remote Sensing Society. He is the recpient of the 1999 IEEE Heinrich Hertz Medal and the 1999 URSI Dellinger Gold Medal. In 2000, he received the IEEE Third Millennium Medal.

John Rhodes Thomas received the B.S. degree in physics from the California Institute of Technology, Pasadena, in 1957 and the M.S.E.E. degree from the University of Washington, Seattle, in 1998. He is currently working toward the Ph.D. degree in the field of negative index media under Prof. A. Ishimaru.

He was with The Boeing Company from 1958 until retirement in mid1995. From 1973 to 1995, his work was devoted mostly to electromagnetic pulse hardening of aircraft and weapon systems.

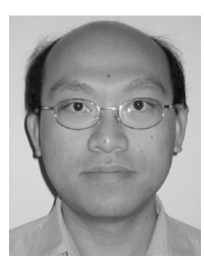

Sermsak Jaruwatanadilok received the B.E. degree in telecommunication engineering from King Mongkut's Institute of Technology Ladkrabang, Thailand, in 1994, the M.S. degree in electrical engineering from Texas A&M University, College Station, in 1997, and the Ph.D. degree in electrical engineering from the University of Washington, Seattle, in 2003.

He is currently with the University of Washington, Seattle. His research interests are optical wave propagation and imaging in random medium, as well as optical and microwave remote sensing.